ACS OMEGA

http://pubs.acs.org/journal/acsodf

Article

# Triazine-Based Conjugated Microporous Polymers for Efficient Hydrogen Production

Wenbo Hao, Renzeng Chen, Yue Zhang, Yuancheng Wang,* and Yingjie Zhao*

Cite This: *ACS Omega* 2021, 6, 23782−23787

Read Online

ACCESS | Metrics & More | Article Recommendations | Supporting Information

**ABSTRACT:** Developing visible-light-active porous organic polymers with high photocatalytic efficiency is highly desirable. Here, two triazine-based conjugated microporous polymers were synthesized. The structures were controllably adjusted to explore the structure−photocatalytic activity relationship. **T-CMP-1** containing more triazine units exhibited a hydrogen evolution rate of 3214.3 $\mu$mol $h^{-1}$ $g^{-1}$, much higher than that of **T-CMP-2** (242.1 $\mu$mol $h^{-1}$ $g^{-1}$). The increasing contents of triazine units bring better hydrogen evolution efficiency.

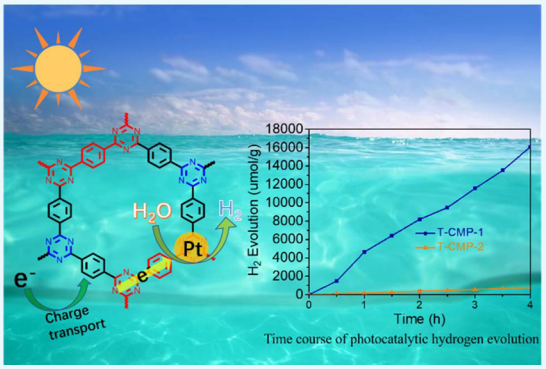


## INTRODUCTION

Hydrogen as a green and sustainable energy has been regarded as an ideal clean fuel.[1] The most promising route for generating hydrogen is direct photocatalytic water splitting.[2,3] In the past few decades, various materials including inorganic semiconducting materials[4−10] and organic polymers[3,11−19] have achieved great progress in photocatalytic hydrogen evolution. However, many of these photocatalysts exhibited poor photoactivity under visible light, whereas solar energy mainly lies in the visible and infrared regions.[3,20] In recent years, conjugated organic polymers as photocatalysts have drawn much attention owing to their tunable structure, electronic properties, and bandgaps, which enable them to harvest as much visible light as to realize highly efficient photocatalytic hydrogen evolution.[3,21−23]

Conjugated microporous polymers (CMPs) are a class of organic porous polymers that combine $\pi$-conjugated skeletons and porous structures.[24−28] Compared with other non-$\pi$-conjugated porous materials or conventional nonporous 1D conjugated polymers, CMPs often exhibit exceptional properties. They allow the complementary utilization of $\pi$-conjugated skeletons and nanoporous characteristics for functional exploration. Benefiting from their unique conjugated and porous structures, CMPs have shown great potential for challenging energy and environmental issues, such as gas storage and separation,[29−32] heterogeneous catalysis,[33−35] optoelectronics,[36−39] and energy storage.[40,41] The large electron delocalized structure and tunable optoelectronic properties of CMPs can facilitate charge transport in the molecular framework, which makes it suitable for photocatalytic hydrogen evolution.[23,42] The structural diversities and the adjustabilities of the organic CMP materials provide a platform to formulate the structure−property relationship.[25] Here, we attempted to synthesize triazine-ring-based CMP materials by one-step polycondensation, which is a simple and convenient method for preparing CMP materials. By slightly changing the structure of the monomers, two CMPs with different contents of triazine units were synthesized successfully. The semiconductor properties of the two CMPs were systemically characterized. Furthermore, photocatalytic water splitting was also employed to verify the effect of the nitrogen atom content on photocatalytic performance. It was found that increasing the triazine units will obviously enhance the photocatalytic performance. **T-CMP-1** exhibits an attractive photocatalytic hydrogen evolution rate (HER) of 3214.3 $\mu$mol $h^{-1}$ $g^{-1}$ under visible-light irradiation, much higher than that of **T-CMP-2**, which has fewer triazine units (242.1 $\mu$mol $h^{-1}$ $g^{-1}$).

## RESULTS AND DISCUSSION

To controllably adjust the contents of triazine units in CMPs, building blocks **A** (2,4,6-tris(4-formylphenyl)-1,3,5-triazine) and **B** (1,3,5-tris(4-formylphenyl)-benzene) with a similar structure were selected as C3 symmetrical monomers. As illustrated in Scheme 1, the two triazine-based CMPs were prepared via one-step polycondensation reactions between **C**

**Received:** May 18, 2021
**Accepted:** July 14, 2021
**Published:** September 8, 2021

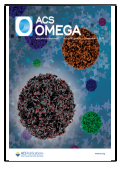

**Scheme 1. Synthesis and Structures of T-CMP-1 and T-CMP-2**

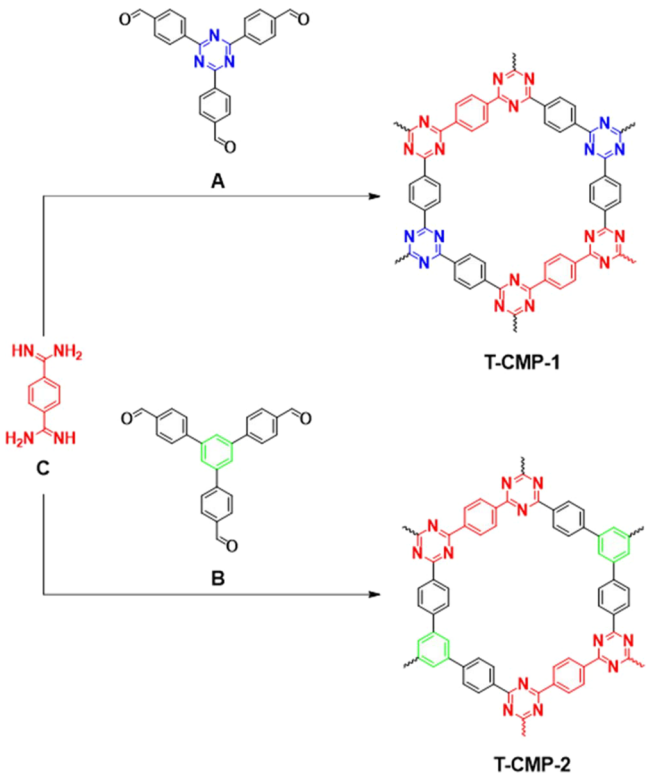


(1,4-benzenedicarboximidamide) and aromatic aldehydes (**A** and **B**) by using sodium methanol as a catalyst at a relatively low temperature (120 °C) (For details, see the Supporting Information). The two CMPs were obtained as yellow solid powder. Both of the as-prepared solid samples are insoluble in common organic solvents. Unfortunately, no sign of crystallinity was observed according to the PXRD results (Figure S1).

The successful preparation of the CMPs was further confirmed by FT-IR spectra. For **T-CMP-2**, the signals at 1590 $cm^{-1}$ were attributed to the −C═N− bonds in triazine, which suggests the formation of triazine units (Figure S2). However, for **T-CMP-1**, the FT-IR signals of the newly formed triazine ring overlapped with those of the triazine in monomer **A**. So, it is difficult to confirm the formation of the triazine ring. In this case, the solid-state cross-polarization magic-angle spinning (CP-MAS) $^{13}C$ NMR spectra were then employed to clarify the successful conversion. As depicted in Figure 1, no obvious difference between these two CMPs was observed from the CP-MAS $^{13}C$ NMR spectra. The peak at 171 ppm further confirmed the formation of a triazine structure, while the peaks at 129 ppm proved the existence of a phenyl ring. All the results above proved successfully the synthesis of **T-CMP-1** and **T-CMP-2** via one-step polycondensation reaction. Thermogravimetric analysis showed that both of these CMPs displayed good thermal stability with decomposition temperatures up to 400 °C (Figure S3).

Nitrogen adsorption−desorption experiments (Figure 2) at 77 K were then performed to evaluate the porosities of the prepared CMPs. Both of **T-CMP-1** and **T-CMP-2** showed typical type IV reversible isotherms, indicating the presence of micropores and mesopores. The Brunauer−Emmett−Teller (BET) surface areas of **T-CMP-1** and **T-CMP-2** were found to be 152.6 and 213.4 $m^2\ g^{-1}$, respectively. According to the pore

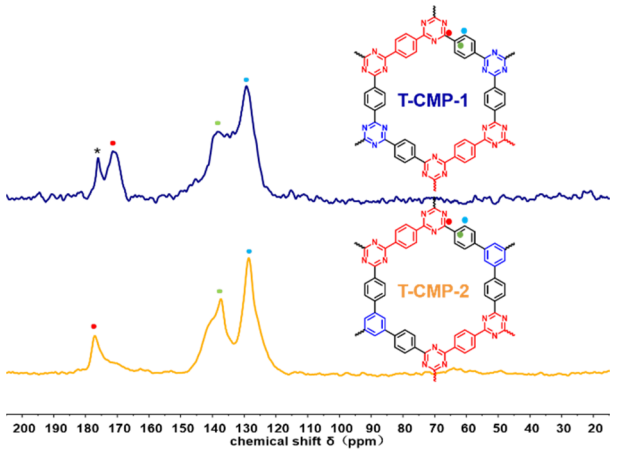


**Figure 1.** $^{13}C$ CP-MAS NMR spectra of **T-CMP-1** and **T-CMP-2**. The residual signal of carboximidamide is marked with an asterisk (*).

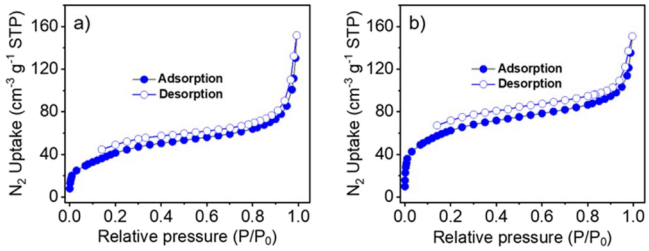


**Figure 2.** $N_2$ adsorption−desorption isotherms (77 K) of **T-CMP-1** (a) and **T-CMP-2** (b).

size distribution analysis, both of the two CMPs mainly consisted of narrow micropores (Figure S4).

The morphologies of **T-CMP-1** and **T-CMP-2** were then studied by scanning electron microscopy (SEM) and transmission electron microscopy (TEM). It is worth noting that the SEM images (Figure 3a,b) show that **T-CMP-1** and **T-CMP-2** possess different morphologies. **T-CMP-1** is composed of relatively regular rectangular particles, while a uniform cube-

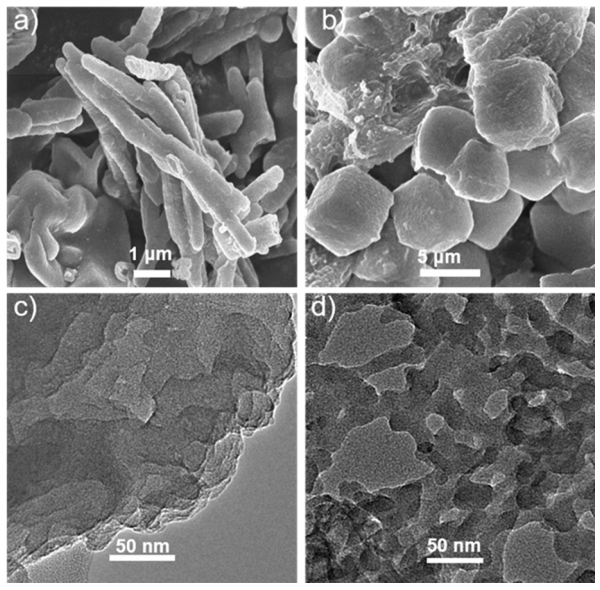


**Figure 3.** SEM and TEM images of **T-CMP-1** (a,c) and **T-CMP-2** (b,d).



https://doi.org/10.1021/acsomega.1c02592
ACS Omega 2021, 6, 23782−23787

like structure was observed in **T-CMP-2**. Obvious layered structures were observed for both of these two CMPs revealed by HRTEM images (Figure 3c,d).

The triazine-rich structures of **T-CMP-1** and **T-CMP-2** evoke our interest to further explore their photocatalytic performance.[43−45] The photocatalytic experiments were performed by suspending the CMP materials in water under irradiation of a 300 W Xe lamp. Ascorbic acid was selected as the optimal sacrificial electron donor for both of the CMPs. As illustrated in Figure 4a, **T-CMP-1** displayed a relatively high

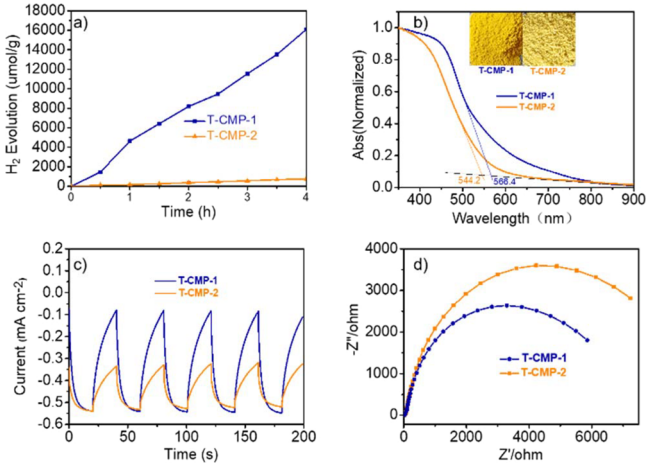


**Figure 4.** (a) Time course of photocatalytic hydrogen evolution for **T-CMP-1** (blue curve) and **T-CMP-2** (orange curve) (>420 nm). (b) Solid-state absorption spectra of **T-CMP-1** and **T-CMP-2**. (c) Periodic on/off photocurrent output of **T-CMP-1** and **T-CMP-2** casted on FTO glass. (d) Electrochemical impedance spectroscopy Nyquist plots for **T-CMP-1** and **T-CMP-2**.

photocatalytic activity with a hydrogen evolution rate (HER) of 3214.3 $\mu$mol h$^{-1}$ g$^{-1}$ under visible light ($\lambda$ > 420 nm). Even under monochromatic-light irradiation, the HER could still reach 1466.9 (420 nm) and 214.2 $\mu$mol h$^{-1}$ g$^{-1}$ (450 nm). Interestingly, for **T-CMP-2**, the HER is only 242.1 $\mu$mol h$^{-1}$ g$^{-1}$ under visible light. Lower HERs of 119.6 (420 nm) and 9.56 $\mu$mol h$^{-1}$ g$^{-1}$ (450 nm) were observed under monochromatic-light irradiation. According to the results of photocatalysis, the apparent quantum yields (AQYs) of **T-CMP-1** (5 mg) were measured to be 0.890 and 0.437% at 420 and 450 nm, respectively. Meanwhile, the AQYs of **T-CMP-2** were 0.122 and 0.0319% at 420 and 450 nm, respectively. Benefiting from the metal-free synthesis method (e.g., Pt and Pd), the enormous differences of the HER and the AQY were clearly attributed to the structural difference.

To explore the essential reasons for the dramatic difference in the photocatalytic performance of **T-CMP-1** and **T-CMP-2**, the solid-state absorption spectra were first measured to study the photophysical properties of these two CMPs. As shown in Figure 4b, the absorptions of the two CMPs were found to cover almost the entire visible-light region extended to 800 nm. Thus, both of the two CMPs have the potential to harvest visible light for photocatalytic hydrogen evolution. According to the absorption spectra, the bandgaps of **T-CMP-1** and **T-CMP-2** are calculated to be 2.19 and 2.28 eV, respectively. No obvious difference was observed in the bandgaps. The cyclic voltammetry measurements were then performed to evaluate the energy levels (Figure S5). The lowest unoccupied molecular orbital (LUMO) and the highest occupied molecular orbital (HOMO) energy levels of **T-CMP-2** were measured to be −3.69 and − 5.97 eV, respectively. For **T-CMP-1**, a similar LUMO energy level of −3.74 eV and a HOMO energy level of −5.93 eV were obtained. These data suggest that **T-CMP-1** is prone to generating holes under visible-light irradiation. The photocurrent measurements were also performed to evaluate the separation efficiency of the photoinduced electron−hole pairs. As depicted in Figure 4c, the photocurrent response of the **T-CMP-1** electrode was higher than that of the **T-CMP-2** electrode under visible light, which was consistent with the photocatalytic activity. Furthermore, electrochemical impedance spectroscopy suggests that **T-CMP-1** possessed a better electronic conductivity than **T-CMP-2** (Figure 4d). These results demonstrated that the performance of photocatalysis can be greatly improved with the increase of the triazine unit, and the absorption and utilization of visible light can be improved (Figure 4b). A photocatalytic stability test of **T-CMP-1** was also performed (Figure S6). No obvious decrease in the photocatalytic performance was observed after three cycles.

## CONCLUSIONS

In summary, we have successfully designed and synthesized two triazine-based CMPs with different contents of triazine units. The subtle structural variation leads to an enormous difference in photocatalytic performance. **T-CMP-1** exhibited an HER of 3214.3 $\mu$mol h$^{-1}$ g$^{-1}$ under visible-light irradiation, while the HER of **T-CMP-2** only reached 242.1 $\mu$mol h$^{-1}$ g$^{-1}$. As a result, the photocatalytic performance could be greatly improved by increasing the content of the triazine units in CMPs. These results provide a strategy for the design of conjugated organic porous polymers with high photocatalytic performance for solar-energy-driven hydrogen evolution.

## EXPERIMENTAL SECTION

**Materials.** Unless otherwise stated, all other reagents were purchased commercially and can be used without further purification. Organic solvents including ethanol, dichloromethane (DCM), petroleum ether, ethyl acetate, acetone, *N*,*N*-dimethylformamide (DMF), tetrahydrofuran, ascorbic acid, and diluted hydrochloric acid were purchased from Yantai Far East Fine Chemical Co., Ltd. All aqueous solutions were prepared with Milli-Q water.

**Instruments and Methods.** $^{1}$H and $^{13}$C NMR spectra were measured on 400 MHz spectrometers (Bruker AVANCE NEO 400 Ascend) in the indicated solvents at room temperature. High-resolution solid-state NMR spectra were recorded on an Agilent NMR spectrometer (60054-ASC) using a standard CP pulse sequence probe with 4 mm (outside diameter) zirconia rotors.

TGA was carried out in a nitrogen atmosphere using a TA-Q20 in the United States. The test condition was that the temperature was raised from room temperature to 800 °C and the rate was 10 °C/min. There was no equilibrium delay.

Scanning electron microscope (SEM) images were collected using a scanning electron microscope (JEOL, JSM-7500F) at an accelerating voltage of 5.0 kV. Transmission electron microscopy (TEM) was performed on a JEM-2100 electron microscope with an accelerating voltage of 200 kV. Solid-state UV−vis absorbance was measured using a UV spectrophotometer (HITACHI, U-3900).


https://doi.org/10.1021/acsomega.1c02592
ACS Omega 2021, 6, 23782−23787

Powder X-ray diffraction (PXRD) patterns were obtained on a PANalytical Empyrean X-ray diffractometer with Cu K$\alpha$ line-focused radiation at 40 kV and 40 mA from $2\theta$ = 1.5 up to 20° with a 0.02° increment by Bragg−Brentano. The powdered sample was added to the glass and compacted for measurement.

$N_2$ adsorption isotherms were measured up to 1 bar at 77 K using a Micrometrics ASAP 2460 surface area analyzer. Prior to measurements, samples (ca. 100 mg) were degassed for over 12 h at 120 °C. Ultrahigh-purity-grade $N_2$ and He were used throughout the adsorption experiments. Oil-free vacuum pumps and oil-free pressure regulators were used for measurements to prevent contamination of the samples during the degassing process and isotherm measurement.

*General Procedures for Photocurrent Measurements.* Photocurrent measurements were performed on a CHI 760E electrochemical system (Shanghai, China), using indium fluorine-doped oxide-coated glass slides as the working electrode, Ag/AgCl as the reference electrode, and a platinum wire as the counter electrode in a three-electrode system. The mixed binder solution is made up of 75 $\mu$L of a polytetrafluoroethylene emulsion and ethanol (675 $\mu$L). The solution was mixed with a polymer (10 mg), the polymer was dispersed by ultrasonication, and the solution (50 $\mu$L) was dropped onto the FTO glass working electrode (active area of 1 $cm^2$). The samples were dried at 50 °C for 30 min. $N_2$ was used to purify the three-electrode system for 5 min before measurement. Measurements were made in a $Na_2SO_4$ solution (0.1 M), and the back of the FTO working electrode was illuminated with a solar simulator (1 sun, ABA-grade).

*General Procedures for Photocatalytic Hydrogen Evolution.* The photocatalytic hydrogen generation experiments of the photocatalysts were performed on a set of photocatalytic equipment (Beijing Perfect Light Co.). First of all, the as-synthesized polymer of 5 mg was ultrasonically dispersed in 0.1 M ascorbic acid to form a well-dispersed polymer suspension. $H_2PtCl_6$ (20 $\mu$L, 8 wt %) was then added to the reaction system. After the photocatalytic system was degassed to remove the dissolved air, the suspension was irradiated with a 300 W Xe lamp under vacuum with stirring. Circulating cooling water was used to keep the photocatalytic reaction temperature at 5 °C. A 420 nm filter was used to filter off ultraviolet light to obtain simulated visible-light irradiation ($\lambda$ > 420 nm). The produced hydrogen was measured online by using a gas chromatograph.

## ■ ASSOCIATED CONTENT

### Supporting Information

The Supporting Information is available free of charge at https://pubs.acs.org/doi/10.1021/acsomega.1c02592.

Synthetic procedures, PXRD data, FT-IR, TGA, pore size distribution profiles, CV curves, and cycling tests (Figures S1−S6) (PDF)

## ■ AUTHOR INFORMATION


### Corresponding Authors

**Yuancheng Wang** − *Key Laboratory of Biobased Polymer Materials, Shandong Provincial Education Department, College of Polymer Science and Engineering, Qingdao University of Science and Technology, Qingdao 266042, China;* orcid.org/0000-0002-2915-5941; Email: wangyuancheng@qust.edu.cn

**Yingjie Zhao** − *Key Laboratory of Biobased Polymer Materials, Shandong Provincial Education Department, College of Polymer Science and Engineering, Qingdao University of Science and Technology, Qingdao 266042, China;* orcid.org/0000-0002-2668-3722; Email: yz@qust.edu.cn

### Authors

**Wenbo Hao** − *Key Laboratory of Biobased Polymer Materials, Shandong Provincial Education Department, College of Polymer Science and Engineering, Qingdao University of Science and Technology, Qingdao 266042, China*

**Renzeng Chen** − *Key Laboratory of Biobased Polymer Materials, Shandong Provincial Education Department, College of Polymer Science and Engineering, Qingdao University of Science and Technology, Qingdao 266042, China*

**Yue Zhang** − *Key Laboratory of Biobased Polymer Materials, Shandong Provincial Education Department, College of Polymer Science and Engineering, Qingdao University of Science and Technology, Qingdao 266042, China*

Complete contact information is available at: https://pubs.acs.org/10.1021/acsomega.1c02592


### Notes

The authors declare no competing financial interest.

## ■ ACKNOWLEDGMENTS

This work was supported by the National Natural Science Foundation of China (21905150) and the Natural Science Foundation of Shandong Province (no. ZR2020ZD38).

## ■ REFERENCES


(1) Christoforidis, K. C.; Fornasiero, P. Photocatalytic Hydrogen Production: A Rift into the Future Energy Supply. *ChemCatChem* **2017**, *9*, 1523−1544.

(2) Wang, Z.; Li, C.; Domen, K. Recent developments in heterogeneous photocatalysts for solar-driven overall water splitting. *Chem. Soc. Rev.* **2019**, *48*, 2109−2125.

(3) Dai, C.; Liu, B. Conjugated polymers for visible-light-driven photocatalysis. *Energy Environ. Sci.* **2020**, *13*, 24−52.

(4) Okamoto, Y.; Ida, S.; Hyodo, J.; Hagiwara, H.; Ishihara, T. Synthesis and Photocatalytic Activity of Rhodium-Doped Calcium Niobate Nanosheets for Hydrogen Production from a Water/Methanol System without Cocatalyst Loading. *J. Am. Chem. Soc.* **2011**, *133*, 18034−18037.

(5) Liu, M.; Chen, Y.; Su, J.; Shi, J.; Wang, X.; Guo, L. Photocatalytic hydrogen production using twinned nanocrystals and an unanchored $NiS_x$ co-catalyst. *Nat. Energy* **2016**, *1*, 16151.

(6) Zhou, X.; Liu, N.; Schmidt, J.; Kahnt, A.; Osvet, A.; Romeis, S.; Zolnhofer, E. M.; Marthala, V. R. R.; Guldi, D. M.; Peukert, W.; Hartmann, M.; Meyer, K.; Schmuki, P. Noble-Metal-Free Photocatalytic Hydrogen Evolution Activity: The Impact of Ball Milling Anatase Nanopowders with $TiH_2$. *Adv. Mater.* **2017**, *29*, 1604747.

(7) Gopannagari, M.; Kumar, D. P.; Reddy, D. A.; Hong, S.; Song, M. I.; Kim, T. K. In situ preparation of few-layered $WS_2$ nanosheets and exfoliation into bilayers on CdS nanorods for ultrafast charge carrier migrations toward enhanced photocatalytic hydrogen production. *J. Catal.* **2017**, *351*, 153−160.

(8) Ida, S.; Ishihara, T. Recent Progress in Two-Dimensional Oxide Photocatalysts for Water Splitting. *J. Phys. Chem. Lett.* **2014**, *5*, 2533−2542.

(9) Hisatomi, T.; Kubota, J.; Domen, K. Recent advances in semiconductors for photocatalytic and photoelectrochemical water splitting. *Chem. Soc. Rev.* **2014**, *43*, 7520−7535.

(10) Chandrasekaran, S.; Yao, L.; Deng, L.; Bowen, C.; Zhang, Y.; Chen, S.; Lin, Z.; Peng, F.; Zhang, P. Recent advances in metal sulfides: from controlled fabrication to electrocatalytic, photocatalytic and photoelectrochemical water splitting and beyond. *Chem. Soc. Rev.* **2019**, *48*, 4178−4280.
(11) Sachs, M.; Sprick, R. S.; Pearce, D.; Hillman, S. A. J.; Monti, A.; Guilbert, A. A. Y.; Brownbill, N. J.; Dimitrov, S.; Shi, X.; Blanc, F.; Zwijnenburg, M. A.; Nelson, J.; Durrant, J. R.; Cooper, A. I. Understanding structure-activity relationships in linear polymer photocatalysts for hydrogen evolution. *Nat. Commun.* **2018**, *9*, 4968−4968.
(12) Li, L.; Cai, Z.; Wu, Q.; Lo, W.-Y.; Zhang, N.; Chen, L. X.; Yu, L. Rational Design of Porous Conjugated Polymers and Roles of Residual Palladium for Photocatalytic Hydrogen Production. *J. Am. Chem. Soc.* **2016**, *138*, 7681−7686.
(13) Wang, X.; Maeda, K.; Thomas, A.; Takanabe, K.; Xin, G.; Carlsson, J. M.; Domen, K.; Antonietti, M. A metal-free polymeric photocatalyst for hydrogen production from water under visible light. *Nat. Mater.* **2009**, *8*, 76−80.
(14) Wang, Y.; Silveri, F.; Bayazit, M. K.; Ruan, Q.; Li, Y.; Xie, J.; Catlow, C. R. A.; Tang, J. Bandgap Engineering of Organic Semiconductors for Highly Efficient Photocatalytic Water Splitting. *Adv. Energy Mater.* **2018**, *8*, 1801084.
(15) Wang, N.; Cheng, G.; Guo, L.; Tan, B.; Jin, S. Hollow Covalent Triazine Frameworks with Variable Shell Thickness and Morphology. *Adv. Funct. Mater.* **2019**, *29*, 1904781.
(16) Wang, K.; Yang, L.-M.; Wang, X.; Guo, L.; Cheng, G.; Zhang, C.; Jin, S.; Tan, B.; Cooper, A. Covalent Triazine Frameworks via a Low-Temperature Polycondensation Approach. *Angew. Chem., Int. Ed.* **2017**, *56*, 14149−14153.
(17) Biswal, B. P.; Vignolo-González, H. A.; Banerjee, T.; Grunenberg, L.; Savasci, G.; Gottschling, K.; Nuss, J.; Ochsenfeld, C.; Lotsch, B. V. Sustained Solar $H_2$ Evolution from a Thiazolo[5,4-*d*]thiazole-Bridged Covalent Organic Framework and Nickel-Thiolate Cluster in Water. *J. Am. Chem. Soc.* **2019**, *141*, 11082−11092.
(18) Banerjee, T.; Haase, F.; Savasci, G.; Gottschling, K.; Ochsenfeld, C.; Lotsch, B. V. Single-Site Photocatalytic $H_2$ Evolution from Covalent Organic Frameworks with Molecular Cobaloxime Co-Catalysts. *J. Am. Chem. Soc.* **2017**, *139*, 16228−16234.
(19) Wang, X.; Chen, L.; Chong, S. Y.; Little, M. A.; Wu, Y.; Zhu, W.-H.; Clowes, R.; Yan, Y.; Zwijnenburg, M. A.; Sprick, R. S.; Cooper, A. I. Sulfone-containing covalent organic frameworks for photocatalytic hydrogen evolution from water. *Nat. Chem.* **2018**, *10*, 1180−1189.
(20) Tee, S. Y.; Win, K. Y.; Teo, W. S.; Koh, L.-D.; Liu, S.; Teng, C. P.; Han, M.-Y. Recent Progress in Energy-Driven Water Splitting. *Adv. Sci.* **2017**, *4*, 1600337.
(21) Sprick, R. S.; Jiang, J.-X.; Bonillo, B.; Ren, S.; Ratvijitvech, T.; Guiglion, P.; Zwijnenburg, M. A.; Adams, D. J.; Cooper, A. I. Tunable Organic Photocatalysts for Visible-Light-Driven Hydrogen Evolution. *J. Am. Chem. Soc.* **2015**, *137*, 3265−3270.
(22) Wang, Z.; Yang, X.; Yang, T.; Zhao, Y.; Wang, F.; Chen, Y.; Zeng, J. H.; Yan, C.; Huang, F.; Jiang, J.-X. Dibenzothiophene Dioxide Based Conjugated Microporous Polymers for Visible-Light-Driven Hydrogen Production. *ACS Catal.* **2018**, *8*, 8590−8596.
(23) Sprick, R. S.; Bai, Y.; Guilbert, A. A. Y.; Zbiri, M.; Aitchison, C. M.; Wilbraham, L.; Yan, Y.; Woods, D. J.; Zwijnenburg, M. A.; Cooper, A. I. Photocatalytic Hydrogen Evolution from Water Using Fluorene and Dibenzothiophene Sulfone-Conjugated Microporous and Linear Polymers. *Chem. Mater.* **2019**, *31*, 305−313.
(24) Chaoui, N.; Trunk, M.; Dawson, R.; Schmidt, J.; Thomas, A. Trends and challenges for microporous polymers. *Chem. Soc. Rev.* **2017**, *46*, 3302−3321.
(25) Lee, J.-S. M.; Cooper, A. I. Advances in Conjugated Microporous Polymers. *Chem. Rev.* **2020**, *120*, 2171−2214.
(26) Xu, Y.; Jin, S.; Xu, H.; Nagai, A.; Jiang, D. Conjugated microporous polymers: design, synthesis and application. *Chem. Soc. Rev.* **2013**, *42*, 8012−8031.
(27) Das, S.; Heasman, P.; Ben, T.; Qiu, S. Porous Organic Materials: Strategic Design and Structure−Function Correlation. *Chem. Rev.* **2017**, *117*, 1515−1563.
(28) Qian, Z.; Wang, Z. J.; Zhang, K. A. I. Covalent triazine frameworks as emerging heterogeneous photocatalysts. *Chem. Mater.* **2021**, *33*, 1909−1926.
(29) Lu, W.; Yuan, D.; Zhao, D.; Schilling, C. I.; Plietzsch, O.; Muller, T.; Bräse, S.; Guenther, J.; Blümel, J.; Krishna, R.; Li, Z.; Zhou, H.-C. Porous Polymer Networks: Synthesis, Porosity, and Applications in Gas Storage/Separation. *Chem. Mater.* **2010**, *22*, 5964−5972.
(30) Dawson, R.; Cooper, A. I.; Adams, D. J. Nanoporous organic polymer networks. *Prog. Polym. Sci.* **2012**, *37*, 530−563.
(31) Dawson, R.; Stöckel, E.; Holst, J. R.; Adams, D. J.; Cooper, A. I. Microporous organic polymers for carbon dioxide capture. *Energy Environ. Sci.* **2011**, *4*, 4239−4245.
(32) Yuan, Y.; Huang, H.; Chen, L.; Chen, Y. *N*,*N*′-Bicarbazole: A Versatile Building Block toward the Construction of Conjugated Porous Polymers for $CO_2$ Capture and Dyes Adsorption. *Macromolecules* **2017**, *50*, 4993−5003.
(33) Jiang, J.-X.; Li, Y.; Wu, X.; Xiao, J.; Adams, D. J.; Cooper, A. I. Conjugated Microporous Polymers with Rose Bengal Dye for Highly Efficient Heterogeneous Organo-Photocatalysis. *Macromolecules* **2013**, *46*, 8779−8783.
(34) Pan, L.; Xu, M.-Y.; Feng, L.-J.; Chen, Q.; He, Y.-J.; Han, B.-H. Conjugated microporous polycarbazole containing tris(2-phenylpyridine)iridium(iii) complexes: phosphorescence, porosity, and heterogeneous organic photocatalysis. *Polym. Chem.* **2016**, *7*, 2299−2307.
(35) Lan, F.; Wang, Q.; Chen, H.; Chen, Y.; Zhang, Y.; Huang, B.; Liu, H.; Liu, J.; Li, R. Preparation of hydrophilic conjugated microporous polymers for efficient visible light-driven nicotinamide adenine dinucleotide regeneration and photobiocatalytic formaldehyde reduction. *ACS Catal.* **2020**, *10*, 12976−12986.
(36) Liu, X.; Xu, Y.; Jiang, D. Conjugated Microporous Polymers as Molecular Sensing Devices: Microporous Architecture Enables Rapid Response and Enhances Sensitivity in Fluorescence-On and Fluorescence-Off Sensing. *J. Am. Chem. Soc.* **2012**, *134*, 8738−8741.
(37) Xu, Y.; Chen, L.; Guo, Z.; Nagai, A.; Jiang, D. Light-Emitting Conjugated Polymers with Microporous Network Architecture: Interweaving Scaffold Promotes Electronic Conjugation, Facilitates Exciton Migration, and Improves Luminescence. *J. Am. Chem. Soc.* **2011**, *133*, 17622−17625.
(38) Xu, Y.; Nagai, A.; Jiang, D. Core−shell conjugated microporous polymers: a new strategy for exploring color-tunable and -controllable light emissions. *Chem. Commun.* **2013**, *49*, 1591−1593.
(39) Jiang, J.-X.; Trewin, A.; Adams, D. J.; Cooper, A. I. Band gap engineering in fluorescent conjugated microporous polymers. *Chem. Sci.* **2011**, *2*, 1777−1781.
(40) Lee, J.-S. M.; Wu, T.-H.; Alston, B. M.; Briggs, M. E.; Hasell, T.; Hu, C.-C.; Cooper, A. I. Porosity-engineered carbons for supercapacitive energy storage using conjugated microporous polymer precursors. *J. Mater. Chem. A* **2016**, *4*, 7665−7673.
(41) Xu, F.; Chen, X.; Tang, Z.; Wu, D.; Fu, R.; Jiang, D. Redox-active conjugated microporous polymers: a new organic platform for highly efficient energy storage. *Chem. Commun.* **2014**, *50*, 4788−4790.
(42) Xiao, W.-J.; Wang, Y.; Wang, W.-R.; Li, J.; Wang, J.; Xu, Z.-W.; Li, J.; Yao, J.; Li, W.-S. Diketopyrrolopyrrole-Based Donor−Acceptor Conjugated Microporous Polymers for Visible-Light-Driven Photocatalytic Hydrogen Production from Water. *Macromolecules* **2020**, *53*, 2454−2463.
(43) Wang, Y.; Liu, H.; Pan, Q.; Ding, N.; Yang, C.; Zhang, Z.; Jia, C.; Li, Z.; Liu, J.; Zhao, Y. Construction of Thiazolo[5,4-*d*]thiazole-based Two-Dimensional Network for Efficient Photocatalytic $CO_2$ Reduction. *ACS Appl. Mater. Interfaces* **2020**, *12*, 46483−46489.
(44) Wang, Y.; Liu, H.; Pan, Q.; Wu, C.; Hao, W.; Xu, J.; Chen, R.; Liu, J.; Li, Z.; Zhao, Y. Construction of Fully Conjugated Covalent Organic Frameworks via Facile Linkage Conversion for Efficient Photoenzymatic Catalysis. *J. Am. Chem. Soc.* **2020**, *142*, 5958−5963.


https://doi.org/10.1021/acsomega.1c02592
*ACS Omega* 2021, 6, 23782−23787

(45) Zhao, Y.; Liu, H.; Wu, C.; Zhang, Z.; Pan, Q.; Hu, F.; Wang, R.; Li, P.; Huang, X.; Li, Z. Fully Conjugated Two-Dimensional $sp^2$-Carbon Covalent Organic Frameworks as Artificial Photosystem I with High Efficiency. *Angew. Chem., Int. Ed.* **2019**, *58*, 5376−5381.



https://doi.org/10.1021/acsomega.1c02592
*ACS Omega* 2021, 6, 23782−23787